

Antibacterial film with chitosan-cinnamaldehyde Schiff base: Fabrication and application in chilled mutton preservation

Lei Wen, Pengfei Du, Weiting Wang, Yaobo Liu, Peng Hu, Jianfang Cao, Yanli Ma *

Institute of Food & Nutrition Science and Technology, Shandong Academy of Agricultural Sciences, Jinan 250100, China

ARTICLE INFO

Keywords:

Natural bacteriostat
Chitosan-Cinnamaldehyde Schiff base
Responsive release
Mutton preservation
Antibacterial packaging

ABSTRACT

Release in response to stimuli such as enzyme, pH, temperature, and light effectively reduces the loss of volatile active compounds and controls the release of active ingredients. In this study, a Schiff base imine bond was formed between chitosan and cinnamaldehyde under mild conditions, and a pH-sensitive antimicrobial film was prepared using a chitosan matrix. The mechanical and physical properties, structure, and amount of cinnamaldehyde release from the chitosan-cinnamaldehyde Schiff base film were analysed, confirming the formation of a chitosan-cinnamaldehyde Schiff base. The film demonstrated good physical properties as well as pH-responsive sensitive release properties with excellent antimicrobial activity. Experiments on the freshness preservation of chilled mutton wrapped in the chitosan-cinnamaldehyde Schiff base film showed that the film can extend the preservation time at 4 °C for up to 4 days, demonstrating good water retention. This film accomplished the controlled release of cinnamaldehyde, meeting the requirements for meat preservation. Thus, the chitosan-cinnamaldehyde Schiff base film can be used as an eco-friendly, smart, responsive, controlled-release packaging material for chilled mutton.

1. Introduction

With the rise in animal diseases and evolving consumer consumption patterns, chilled meat has gradually dominated the mass meat market (Ren, et al., 2022). Because chilled meat is stored consistently in a low-temperature environment that does not fully suppress microbial growth, its shelf life is reduced; thus, widespread commercial distribution is challenging ((Tao et al., 2021)).

Advancements in food preservation have led to the extension of the storage duration of chilled mutton and its derivatives through a combination of diverse physical treatments, innovative packaging approaches, and application of specific chemical additives (Arokiyaraj, et al., 2023; Smaoui et al., 2021). Nonetheless, the use of synthetic chemicals raises concerns related to consumer health (Manzoor, et al., 2023). Over the last few decades, there has been an increasing interest in natural preservatives (Awad et al., 2022). The utilisation of natural bioactive substances in the meat industry is a valuable approach for retarding the oxidation of meat and its related products (Mills et al., 2014). According to our previous research, cinnamaldehyde was a targeted natural antibacterial agent against the dominant spoilage microorganisms in chilled mutton during storage. Cinnamaldehyde, which is a

crucial natural preservative, is a class of natural benzaldehyde compounds found in essential oils such as cinnamon oil, cassia oil, oregano oil, hyacinth oil, and rose oil (Cheng et al., 2023). Regulatory bodies, such as the U.S. Food and Drug Administration (FDA) and the Flavor and Extract Manufacturers Association (FEMA), have categorised cinnamaldehyde as a secure food additive (Sun et al., 2021); there have also been reports of its application as a preservative for meat and meat products (Cavalcante et al., 2023). Previous studies have achieved the abovementioned functions by using films with high antibacterial activity, such as polysaccharide films of chitosan-cinnamaldehyde nanoparticles, cinnamaldehyde cornstarch films and chitosan/alginate dialdehyde trilayer films (Dong et al., 2024; Mondéjar-López et al., 2024). The primary advantage of using cinnamaldehyde as a preservative lies in its ability to have direct contact with the surrounding environment and its high volatility; these properties can be leveraged to create a gaseous phase that induces bacteriostatic effects (Culas et al., 2023). Because of these characteristics, cinnamaldehyde has been used in various methods, including impregnation, coating, fumigation, and slow solid release (J. Zhang et al., 2023). However, the general embedding process, such as microencapsulation, lacks the capability to regulate the release of active ingredients based on specific requirements.

* Corresponding author at: Institute of Food & Nutrition Science and Technology, Shandong Academy of Agricultural Sciences, Jinan 250100, China.
E-mail address: dr_mayanli@163.com (Y. Ma).

The release occurs independently of any alterations in food quality or packaging environment, with the active ingredient diminishing rapidly over time (Batiha et al., 2021). This controlled-release approach also suffers from the drawback of the early depletion of active substances, leading to a reduction of antimicrobial efficiency (Wang et al., 2023). Hence, it is crucial to ensure the stability of cinnamon essential oil and establish a correlation between the release characteristics of cinnamaldehyde and the requirements of meat preservation toward realising efficient preservation of chilled meat (He et al., 2021; J. Zhang et al., 2023).

During the slaughter process, when body cells no longer receive oxygen from the blood, mutton starts to engage in anaerobic respiration, leading to the production of a compound known as lactic acid. Under certain conditions, mutton breaks down lactic acid into carbon dioxide, water, and alcohol, which are then volatilised. Concurrently, enzymes catalyse the breakdown of large molecule adenosine triphosphate in mutton cells into nucleosides, causing a shift in the pH of meat that facilitates the complete decomposition and elimination of metabolic substances (M. Zhang et al., 2024). Simultaneously, bacteria, fungi, and other microorganisms initiate the decomposition of organic materials, resulting in the production of carbon dioxide as one of a metabolic byproduct. The gradual accumulation of carbon dioxide inside the packaging leads to the formation of a slightly acidic environment (Limbo et al., 2013). The imine bond (C=N), known as the Schiff base structure, is formed via condensation between a carbonyl compound and an amino compound (Al Ati et al., 2024). The imine bond withstands neutral and alkaline conditions but readily undergoes hydrolysis in acidic environments (Hou et al., 2023; Wu et al., 2020). Hence, alterations in the pH of the headspace microenvironment resulting from the metabolic release of water and CO₂ from mutton can serve as indicators of the controlled delivery of antibacterial substances.

Schiff bases are commonly synthesised through a condensation reaction between the active amino groups of chitosan and aldehydes/ketones at ambient or reflux temperatures (Heras-Mozos et al., 2023; Negi et al., 2021). Studies have found that Schiff bases can be activated by the acidic environment of fruit juices or vegetables, reducing the number of inoculated pathogens (Lin et al., 2023). Nevertheless, the effect of the Schiff base as a pH-responsive packaging material on the antimicrobial preservation of chilled meat has not yet been elucidated. In our research, we identified the dominant spoilage microorganisms in mutton and selected cinnamaldehyde as a targeted natural antibacterial agent based on its efficacy against the detected microbiota. In this study, we focus on utilising cinnamaldehyde and chitosan to synthesise chitosan-cinnamaldehyde Schiff base via a Schiff base reaction considering the development of an acidic microenvironment in chilled mutton over time. Subsequently, a novel packaging material was fabricated using chitosan as the matrix for film formation, and its antimicrobial properties, mechanical strength, and thermal stability were analysed. Furthermore, through the assessment of various physical and chemical parameters associated with the film applied to chilled mutton during storage, the impact of the antibacterial film on the preservation of chilled mutton was investigated.

2. Materials and methods

2.1. Materials and reagents

Fresh mutton meat was bought from Quanfu Life Plaza. (Jinan, China). Chitosan (95 % deacetylated, MW=200,000) and cinnamaldehyde (with 98 % purity) were obtained from Shanghai Macklin Biochemical Co., Ltd. All reagents were of analytical grade. *Pseudomonas* sp. DSM 17,535, *Brochotrichix* sp. B364, and *Acinetobacter* sp. CCTCC AB 2016,310 were obtained from Ningbo Mingzhou Biotechnology Co., Ltd. *Macrococcus* sp. CICC 24,418 and *Psychrobacter* sp. CICC 24,001 were obtained from the China Center of Industrial Culture Collection (CICC). All the bacterial strains were stored in Luria-Bertani (LB) broth with 25

% glycerol (v/v) at -80 °C. Prior to each experiment, the test strain was shake-cultured in LB broth at 37 °C for 12 h.

2.2. Synthesis of chitosan-cinnamaldehyde Schiff base

The chitosan-cinnamaldehyde Schiff base was obtained according to the method reported by Kuai (Kuai, 2021) with some modifications. Chitosan (3.0 g) was placed in a three-necked flask, followed by the addition of methanol (50 mL) for overnight swelling at room temperature. 10 µL cinnamaldehyde was firstly dissolved in 30 mL anhydrous ethanol, then after thorough mixing, the cinnamaldehyde solution was transferred to a constant pressure dropping funnel and slowly added dropwise to swollen chitosan, with stirring at 45 °C for 8 h. The crude product was filtered, washed with anhydrous ethanol, and subjected to Soxhlet extraction for 12 h, followed by final vacuum drying at 50 °C for 24 h to obtain pale-yellow powdered chitosan-cinnamaldehyde Schiff base.

2.3. Elemental analysis

The content of C and N elements in the chitosan-cinnamaldehyde Schiff base were obtained by an elemental analyzer (Vario EL Cube, Elementar, Germany). The degree of substitution (DS) of chitosan-cinnamaldehyde Schiff base was calculated according to Eq. (1).

$$DS = \frac{M_n R - (8 - 2DD)M_c}{N_c M_c} \quad (1)$$

Where DD is the degree of deacetylation of CS, M_c and M_n are the relative atomic masses of carbon and nitrogen atoms, respectively; N_c and R are the number of carbon atoms and the percentage ratio of carbon and nitrogen content in the substituent molecule, respectively.

2.4. Film preparation

To fabricate the chitosan-cinnamaldehyde Schiff base film (CS-CIN SB), 2 % chitosan was dissolved in a 0.6 % (v/v) acetic acid aqueous solution and stirred at 60 °C for 30 min. Next, the solution was magnetically stirred at 25 °C for 4 h until completely dissolved, with the addition of 0.5 % (v/v) glycerin as a plasticiser. Following this, chitosan-cinnamaldehyde Schiff base with concentrations of 0.45 %, 0.6 %, 0.75 %, 0.9 %, 1.05 %, and 1.2 % (w/v) was then added to the chitosan film solution and homogenized at a speed of 8000 rpm for 3 min. The resultant solution for film formation (100 mL) was then poured onto an acrylic plate and left to air-dry in a forced-air drying box maintained at 40 °C for 24 h. Moreover, cinnamaldehyde film (CIN, with the addition of 0.15 % (w/v) cinnamaldehyde; DS=0.300) and chitosan film (CS, formed using a 2 % chitosan matrix) were prepared via the same procedure and used as the control.

2.5. Inhibitory effect of chitosan-cinnamaldehyde schiff base films

The inhibitory effect of chitosan-cinnamaldehyde Schiff base films were determined using the agar diffusion method (Zhao et al., 2023). A total of 200 µL of bacterial suspension at a concentration of 10⁶-10⁷ CFU/mL was inoculated onto nutrient agar plates and allowed to stand for 15 min. Subsequently, films of different chitosan-cinnamaldehyde Schiff base concentrations were cut into 5 mm diameter discs and carefully placed on the surface of the 90 × 15 mm petri dish. The petri dishes were incubated at 37 °C for 24 h. Subsequently, the diameters of the antimicrobial zones on the plates were assessed. Sterile water was used as the blank control and each sample solution was subjected to three replicates to derive the mean value.

2.6. Cinnamaldehyde release amount of CS-CIN SB in pH buffer solutions

The release amount of CS-CIN SB in pH buffer solutions were determined by the method previously described (Kuai, 2021). An amount of 0.25 g of the CS-CIN SB was accurately weighed and added to 50 mL of acetate-sodium acetate buffer solutions at various pH values. The absorbance values were measured at the maximum absorption wavelength of cinnamaldehyde at 292 nm using a UV spectrophotometer (with three repeated measurements and the average value taken). The sampling intervals during the release process were set at 1.5, 5, 8, 24, 48, 72, and 96 h. The release kinetic curves were calculated on the basis of the standard curve of cinnamaldehyde in the corresponding pH solutions.

2.7. Physical characterisation of films

2.7.1. Thickness

The film thickness was measured using a Vernier caliper (MNT919910, Shanghai, China) with a sensitivity of 0.001 mm. The average thickness was calculated from measurements taken at five random positions.

2.7.3. Mechanical strength

The mechanical strength of the film samples (100 mm × 150 mm) was measured using an automated tensile testing machine (MTSE45.105, Shanghai, China) at ambient temperature. The mechanical strength of the films was determined according to the method described by Hanim (Hanim et al., 2022). The tensile strength (T_s) and elongation at break (EB) of the film samples were calculated using the following equations:

$$T_s(\text{MPa}) = F/b \quad (2)$$

$$\text{EB}(\%) = \Delta L/L_0 \times 100\% \quad (3)$$

where F is the stress at film rupture (N), b is the width of the film (mm), a is the thickness of the film (mm), and L_0 and ΔL are the original length and elongation length of the film sample, respectively (mm).

2.7.4. Water vapour permeability (WVP)

The WVP of the films was determined using a previously described method with slight modifications (Qin et al., 2019). The films (50 mm × 50 mm) were tested to cover a 50 mL polypropylene centrifuge tube (inner diameter = 27 mm) containing silica gel desiccant particles (30 g). The permeation tubes were then placed in a desiccator containing a saturated sodium chloride solution and weighed daily at 25 °C for three consecutive days. WVP was calculated using Eq. (4).

$$\text{WVP} = \Delta m L / (A t \Delta p) \quad (4)$$

where Δm is the change in the weight of the test bottle (g), L is the thickness of each layer of the film (m), A is the exposed area of each film (m²), t is the duration (s), and Δp is the difference in vapour pressure (Pa) ($\Delta p = 1752.09$ Pa).

2.7.5. Moisture content

To determine the moisture content of the films, all film samples were first cut into 20 mm × 20 mm squares, weighed to record the initial weight, and then dried at 105 °C for 24 h until a constant weight was achieved. The moisture content of the film sample was calculated using Eq. (5):

$$\text{Moisture content}(\%) = (M_1 - M_2)/M_1 \times 100\% \quad (5)$$

where M_1 is the initial weight of each film (g) and M_2 is the weight of the film after drying (g).

2.7.6. Water solubility

The water solubility was determined by slightly modifying the method reported by Martínez-Aguilar (Martínez-Aguilar et al. 2023). The initial dry weight of the sample (20 mm × 20 mm film dried at 105 °C for 24 h) was firstly measured, and then immersed in distilled water (50 mL) and stirred at room temperature for 24 h. The insoluble matter was separated through centrifugation at 8000 rpm for 15 min, followed by drying at 105 °C until a constant weight was reached. The water solubility was calculated using Eq. (6).

$$\text{Water solubility}(\%) = (M_1 - M_2)/M_1 \times 100\% \quad (6)$$

where M_1 and M_2 are the initial and final dry weights (g), respectively.

2.7.7. Water contact angle (WCA)

The WCA of the films were measured using a WCA analysis instrument (Dataphysics OCA50, Beijing, China). The film samples (20 mm × 20 mm) were placed on the instrument, and a drop of ultrapure water was dispensed onto the film surface. The moment of droplet contact was captured using a high-definition digital camera.

2.7.8. Scanning electron microscopy (SEM)

The cross-section morphology of the films were observed by a scanning electron microscopy (SU8010, Hitachi High Technologies Corporation, Japan) with an accelerating voltage of 15 keV. All film samples were coated with a thin layer of gold before observation.

2.8. Structural characterisation of films

2.8.1. Fourier transform infrared (FTIR) spectroscopy

Chemical structural characterisation was performed using a Fourier transform infrared spectrometer (Nicolet 6700, Nicolet, USA) to analyse the interactions among the characteristic functional groups. The FTIR spectra of the CS, CIN, and CS-CIN SB and a mixture of cinnamaldehyde and chitosan (1:1; CS+CIN) were measured in the scanning range of 4000–500 cm⁻¹ with a scanning frequency of 32 times min⁻¹.

2.8.2. X-ray diffraction (XRD)

XRD was conducted to determine the crystal structures of the CS, CIN, and CS-CIN SB and evaluate the impact of Schiff base modification on the crystal structure. The films were scanned using an XRD device (D8 ADVANCE A25, Bruker, Germany) in the 2θ range of 5°–65° at room temperature, operating at 40 kV and 40 mA, with a step size of 5°/min.

2.9. Thermogravimetric analysis

Thermal stability is a crucial metric for evaluating the applicability of a material, and the stability of each film was determined through thermogravimetry (TG; Nestal STA 449 F5, Beijing, China) conducted in a nitrogen atmosphere at a flow rate of 20 mL/min (Xie et al., 2023). The films were heated from 25 °C to 800 °C at a heating rate of 10 °C/min.

2.10. Film application for fresh mutton preservation

2.10.1. Sample preparation

Pieces of striploin meat from the underside of mutton vertebral bones were selected and cut. After removing the fat layer and connective tissues on the surface of the mutton meat, the mutton meat was cut into approximately 20 g (20 ± 1 g) samples, totalling 75 samples. The samples were packaged in storage boxes, labelled, and covered with CS, CIN, and CS-CIN SB (size: 150 mm × 150 mm), with a PVC cling film (CK) used as a control. The packaged mutton meat samples were stored in a 4 °C incubator. Samples were taken at 0, 2, 5, 7, 9, 11, and 13 d after packaging to determine the physicochemical and microbiological indicators. Three parallel samples were collected daily for each type of film-wrapped mutton samples for analysis.

2.10.2. Low-field nuclear magnetic resonance (LF-NMR) spectroscopy for relaxation characteristic analysis

The moisture mobility and content of mutton samples was determined using an LF-NMR analyser (NMI20-015V-1, Suzhou, China) (Luan, et al., 2025). A 10 g sample was weighed and placed in a 15 mm glass tube, with an NMR probe inserted into the tube. The proton resonance frequency was set at 23.4 MHz, and relaxation time T_2 was tested using the Carré-Purcell-Meiboom-Gill (CPMG) sequence. Distributed exponential fitting of the CPMG decay curve was performed using the MultiExp Inv Analysis software to calculate the relationship between the relaxation amplitude and time during the relaxation process.

2.10.3. Low-field magnetic resonance imaging (LF-MRI)

A 10 g sample was weighed and placed in a 15 mm glass tube, which was then positioned at the centre of the permanent magnetic coil. The moisture distribution and status were analyzed by pseudocoloring software. The imaging test parameters were set as follows: SF = 20 MHz; TR = 500 ms; TE = 20 ms; slice width = 3.0 mm; slices = 1; average = 2; read size = 256; and phase size=192.

2.10.4. Physicochemical analysis

The pH and total volatile basic nitrogen (TVB-N) of the mutton samples were measured using the method reported by Wang (Wang et al., 2022). The determination of thiobarbituric acid reactive substances (TBARS) was conducted using a thiobarbituric acid enzyme-linked immunosorbent assay (ELISA) kit. The colour parameters of the mutton samples, including L* (lightness/darkness), a* (redness/greenness), and b* (yellowness/blueness), were measured directly on the sample surface using a TS7020 colourimeter (3nh, Shenzhen, China).

The total viable count (TVC) was obtained by modifying the method reported by Ruan et al. (Ruan et al., 2019). 2.2 g meat sample was weighed and homogenized in 20 mL of sterilized normal saline for 30 s, then the 10^{-1} – 10^{-4} dilutions of the homogenate were made. TVC was determined using spread plate technique on standard plate count agar (PCA) after 48 h incubation at 37 °C. The results are expressed as log10 CFU/g.

2.10.5. Analysis of volatile compounds

3 g of minced meat was weighed directly into 20-mL sample vials. A DVB/CAR/PDMS SPME fiber (Supelco Inc., PA, USA) was then introduced into the vial headspace for adsorption of volatile compounds for 20 min within a 60 °C water bath. Following extraction, the fiber was retracted into the needle assembly and immediately transferred to the GC-MS injection port (Agilent 7890B-5977A system) for thermal desorption at 250 °C over 3 min. For the chromatographic separation, the following conditions were used: DB-WAX column (30 m × 0.25 mm × 0.25 µm), high-purity helium as the carrier gas at a flow rate of 1.0 mL/min. The temperature was initially held at 40 °C for 3 min, then increased to 200 °C at 5 °C/min, further raised to 230 °C at 10 °C/min, and finally maintained at 230 °C for 3 min. For mass spectrometric detection, the MS conditions included an electron ionization source with an ionization voltage of 70 eV was used. Both the ion source and the transfer line were maintained at 250 °C. Mass spectra were acquired over a range of 30–400 m/z with a solvent delay of 1 min. Compound identification was achieved by matching acquired mass spectra against the NIST17 mass spectral database (Gaithersburg, Maryland, USA).

2.11. Statistical analysis

Each sample was processed in triplicate, and data graphs were plotted using the Origin 2021 software. The results were expressed as x ± s and analysed via Pearson correlation coefficient analysis with the SPSS software. One-way analysis of variance was conducted for variance analysis, and Duncan's multiple range test was used for the post-hoc

analysis of significant differences ($p < 0.05$).

3. Results and discussion

3.1. Inhibitory effect of chitosan-cinnamaldehyde Schiff base films

The procedure to fabricate the chitosan-cinnamaldehyde Schiff base film is schematically illustrated in Fig. 1A. Owing to the presence of chitosan-cinnamaldehyde Schiff base, CS-CIN SB exhibited inhibitory effect on *Pseudomonas psychrophila*, *Brochothrix thermosphacta*, *Macrococcus caseolyticus*, *Acinetobacter*, and *Psychrobacter cibarius*, which are the main putrefactive bacteria in mutton under refrigeration conditions (Fig. S2), the inhibitory effect on the five bacteria strengthened as the chitosan-cinnamaldehyde Schiff base concentration increased. At a chitosan-cinnamaldehyde Schiff base concentration of 0.75 %, the largest inhibition zone diameter was observed (Fig. 1B), suggesting that chitosan-cinnamaldehyde Schiff base induced the most prominent bacterial inhibition effect at this level of concentration owing to its enhanced diffusion capabilities. As the Schiff base concentration increased, the inhibition zone diameter decreased, suggesting that higher concentrations of cinnamaldehyde led to a diminished inhibitory effect. Enhanced cinnamaldehyde loading may trigger chitosan film restructuring, consequently suppressing molecular mobility and diffusion rates and ultimately diminishing cinnamaldehyde's antimicrobial efficacy. (Chen et al., 2016).

3.2. Release of cinnamaldehyde from CS-CIN SB in pH buffers

Three distinct film samples, CS-CIN SB, CIN, and CS, exhibit specific absorption peaks in the ultraviolet spectrum, with a peak value at 292 nm (Fig. S3A). Additionally, the acid-sensitive imine bonds in CS-CIN SB trigger the release of cinnamaldehyde under acidic conditions (Fig. S3B). The hydrolysis of chitosan-cinnamaldehyde Schiff base was monitored by the release of aldehydes when exposed to buffer solutions with different pH values. Fig. 2A shows the release kinetic curves for CS-CIN SB under various pH conditions. Within 1.5 h, the release of CS-CIN SB in the pH 3 setting exceeded 80 %, indicating the highest release rate of CS-CIN SB at this pH level. Notably, CS-CIN SB exhibited a pronounced release effect in a mildly acidic environment of pH 5, achieving 62 % of its total release within 1.5 h. Over time, the release amount continued to rise gradually, reaching 87 % after 96 h. The abrupt release of CS-CIN SB in the acidic environment can be explained by the sensitivity of the acid-sensitive imine bond to acidity. In cases where pH dropped to 1.0, the release amount was lower than those at pH levels of 3.0 and 5.0. Similar results were observed in cinnamaldehyde-chitosan Schiff base powder (Kuai, 2021). This phenomenon could be attributed to the likelihood that chitosan-cinnamaldehyde Schiff base undergoes a nucleophilic addition reaction in the presence of water molecules under highly acidic conditions, thereby impeding the release of cinnamaldehyde (Heras-Mozos, 2022).

In summary, the acid-sensitive imine bonds in CS-CIN SB exhibited varied release properties under different pH conditions. Thus, CS-CIN SB can adapt to variations in the acidic microenvironment of chilled mutton packaging, enabling dynamic regulation of antimicrobial agent release.

3.3. Physical properties of films

3.3.1. Thickness and mechanical properties of films

As shown in Fig. 2B, the addition of cinnamaldehyde and chitosan-cinnamaldehyde Schiff base led to a significant increase in film thickness (from 0.10 mm to 0.15 mm) ($p < 0.05$). This suggests that the inclusion of chitosan and cinnamaldehyde causes the films to have a more open microstructure, enhancing their roughness and porosity and thus overall thickness.

Fig. 2C shows the mechanical properties of the films. Specifically, the tensile strength of the CIN significantly improved in relation to that of

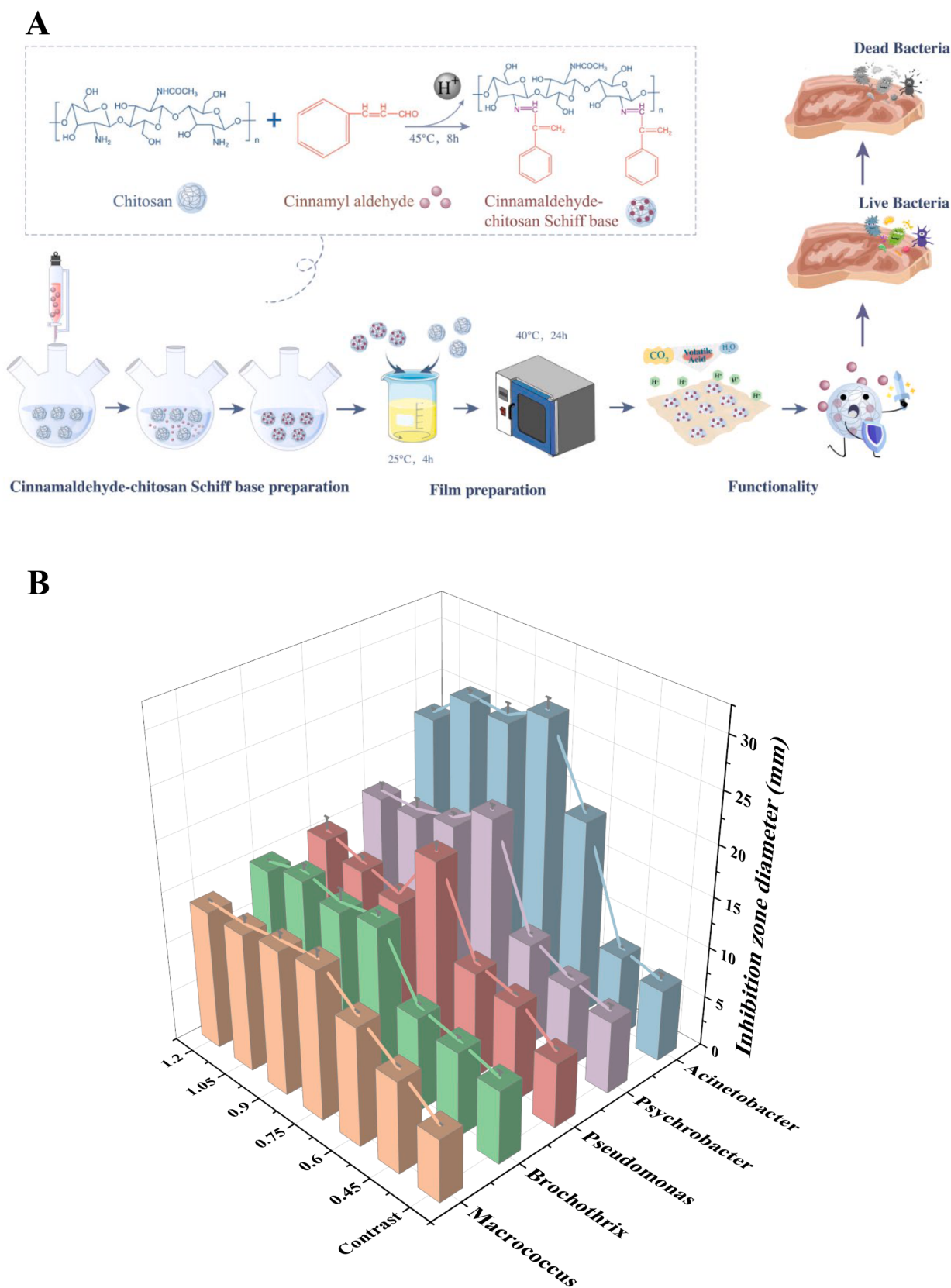


Fig. 1. Schematic illustration of the fabrication process of CS-CIN SB (A); Antibacterial effect of CS-CIN SB with different Schiff base concentrations (B).

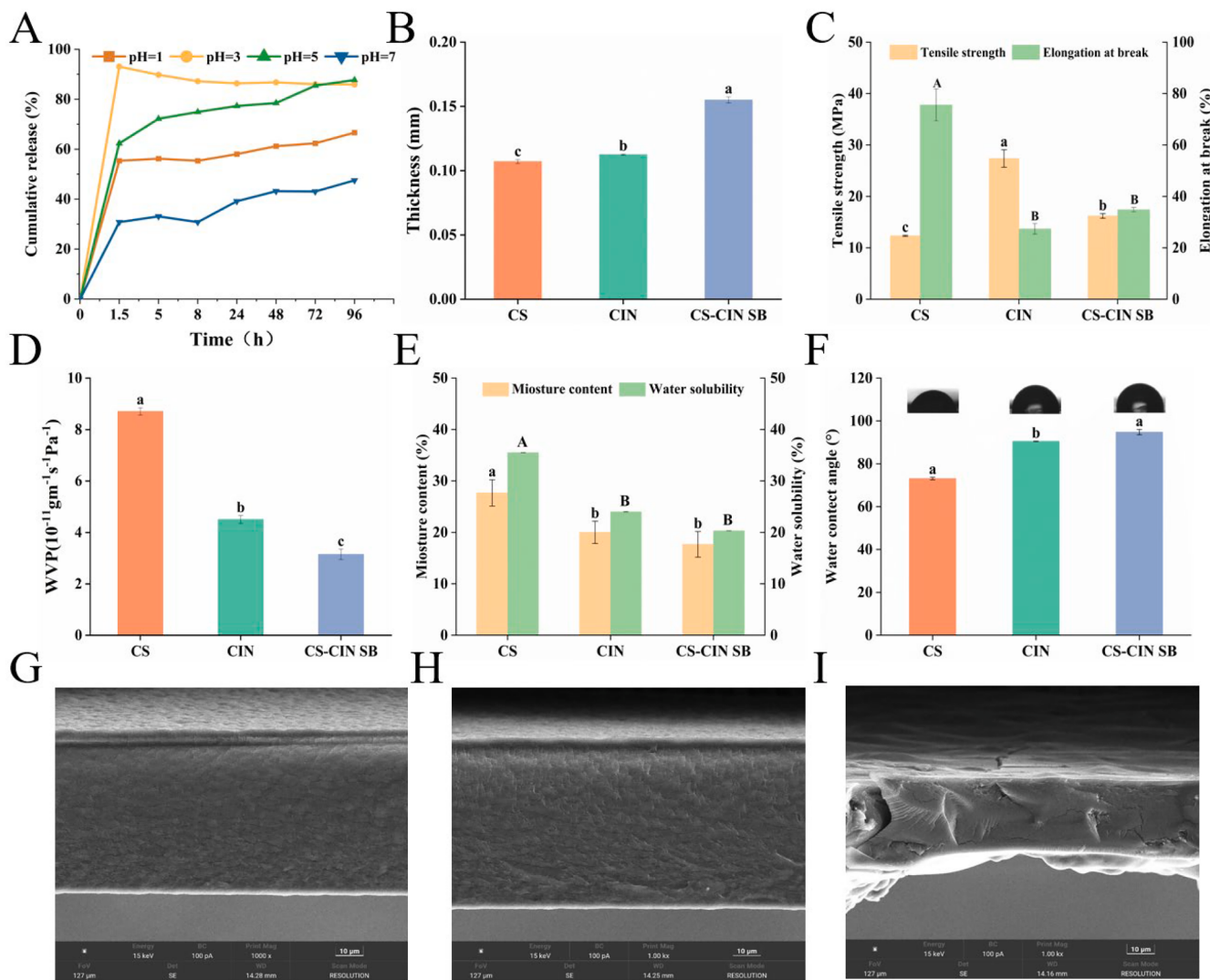


Fig. 2. Release kinetics curves of CS-CIN SB at different pH values (A); Thickness (B); Tensile strength and Elongation at break (C); Water vapour transmittance (D); Moisture content and Water solubility (E); WCA (F) and cross-section images (G-I) of the CS, CIN, and CS-CIN SB. Different letters indicate significant difference ($p < 0.05$).

the other two films ($P < 0.05$). The enhanced tensile strength may be due to increased intermolecular interactions between cinnamaldehyde and chitosan (Khanzada, 2023). On the other hand, this enhancement can be attributed to the presence of the benzene ring in CIN. The benzene ring, composed of six carbon and six hydrogen atoms, is highly stable and has a rigid structure (Wu et al., 2022). The rigidity of this structure limits its rotational freedom in space, maintaining a high level of planarity and resistance to deformation or distortion, thereby ensuring an elevated tensile strength. CS-CIN SB exhibits higher tensile strength than CS because of the incorporation of the benzene ring and rigid imine bond into CS (Khanzada et al., 2023). The lower tensile strength of CS-CIN SB compared to CIN may be due to its rough cross-section. The primary reason for the flexibility of CS is the abundance of σ -single bonds that allow for internal rotation, thereby constraining the tensile strength of CS (Feng et al., 2024). The decrease in elongation of CIN and CS-CIN SB might be due to increasing interactions such as increased hydrogen bonding and crosslinking reactions (Nadira et al., 2022).

3.3.2. WVP

WVP refers to the capability of a substance to transfer moisture to its surroundings or the atmosphere, and serves as a critical parameter for films utilised in packaging (Tao et al., 2021). Fig. 2D shows the WVP of

the CS, CIN, and CS-CIN SB. The WVP values of the CS-CIN SB and CIN were 3.14×10^{-11} and $4.5 \times 10^{-11} \text{ g m}^{-1} \text{s}^{-1} \text{Pa}^{-1}$, respectively, which were lower than those of the CS. This demonstrates that the chemical and structural attributes of the polymer matrix, along with the extent of hydrophobic interactions within the film structure, significantly influence the permeability. Low permeability signifies excellent water barrier properties, preventing the leaching of chitosan-cinnamaldehyde Schiff base from water and enhancing its stability. The CS is a polysaccharide membrane with hydrophilic properties, in which the polar groups ($-OH$) on its chain form hydrogen bonds with water molecules, facilitating their diffusion and eventual disintegration (Tagrida et al., 2023). Through the incorporation of cinnamaldehyde and the formation of imine bonds, hydrophobic benzene rings were introduced, thereby impeding the penetration of water molecules and reducing water molecule permeation. Concurrently, chitosan underwent robust interaction with cinnamaldehyde, resulting in a dense network microstructure that elongated the diffusion path within the network and effectively restrained the diffusion of water molecules.

3.3.3. Moisture content

Fig. 2E shows that the moisture content of the CS peaked at 27.67 %, whereas that of the CIN and CS-CIN SB decreased to 20 % and 17.67 %,

respectively. This difference is due to cinnamaldehyde disrupting the interaction between chitosan and water molecules, resulting in lower moisture content in the film. CS-CIN SB exhibited the lowest hydrophilicity, likely owing to the incorporation of hydrophobic benzene rings during formation. These rings may have reduced the availability of hydrophilic amino groups, resulting in a decrease in the overall hydrophilic character of the corresponding film.

3.3.4. Water solubility

Fig. 2E shows that the water solubility of the CS reached a peak of 35.51 %, whereas that of the CIN and CS-CIN SB significantly decreased ($p < 0.05$). This disparity may be attributed to the stable molecular structure and hydrophobic nature of cinnamaldehyde bearing the benzene ring. Consequently, the addition of cinnamaldehyde or chitosan-cinnamaldehyde Schiff base to the film reduced its water solubility.

3.3.5. WCA

The hydrophilicity of a substance is an intrinsic property because its molecular structure contains polar groups and has a strong affinity for water (Khanegah et al., 2018). As shown in **Fig. 2F**, the WCA value of the CIN increased ($p < 0.05$) to 90.5° due to the presence of hydrophobic cinnamaldehyde. The incorporation of chitosan-cinnamaldehyde Schiff base led to a significant change in WCA compared to CS and CIN. This can be attributed to the formation of an imine bond between the aldehyde group of cinnamaldehyde and the amino group of chitosan, resulting in the consumption of the hydrophilic aldehyde group.

3.3.6. SEM

Fig. 2G-I shows the cross-sections of films. CS was homogenous with a compact and regular continuous matrix. When cinnamaldehyde was incorporated to the chitosan matrix, a coarse microstructure was formed in CIN. Similar results were observed in chitosan-Cinnamon leaf essential oil films (Perdones et al., 2014). The presence of aggregated domains within the CS-CIN SB cross-section reveals suboptimal dispersion homogeneity, necessitating interfacial modulation strategies for improved phase distribution.

3.4. Film characterisation

3.4.1. Fourier transform infrared spectroscopy (FTIR)

Fig. 3A shows the FTIR spectra of the CS, CIN, and CS-CIN SB and a mixture of cinnamaldehyde and chitosan (CS+CIN). The FTIR spectrum of the CS exhibited an amide II (N–H) bending vibration peak at 1597 cm⁻¹, along with a peak corresponding to the stretching vibration of the CS amide I bond (C=O) at 1655 cm⁻¹ (Liu et al., 2017; M. Zhang et al., 2024). Furthermore, the broad band within the range of 3200–3600 cm⁻¹ was ascribed to the stretching vibrations of the multiple absorption peaks attributed to –OH and –NH. The FTIR spectrum of the CIN showed prominent absorption peaks at 1681 cm⁻¹ (C=O bond in the side chain), 1625 cm⁻¹ (C=C bond), and 1495 and 1449 cm⁻¹ (benzene ring backbone). The characteristic peaks of the raw materials persisted in the FTIR spectrum of the CS and CIN mixture, suggesting that the IR spectra of the mixture resulted from the simple superposition of the IR spectra of the two raw materials, with no formation of new chemical groups.

The appearance of the C=N stretching vibration peak in the FTIR

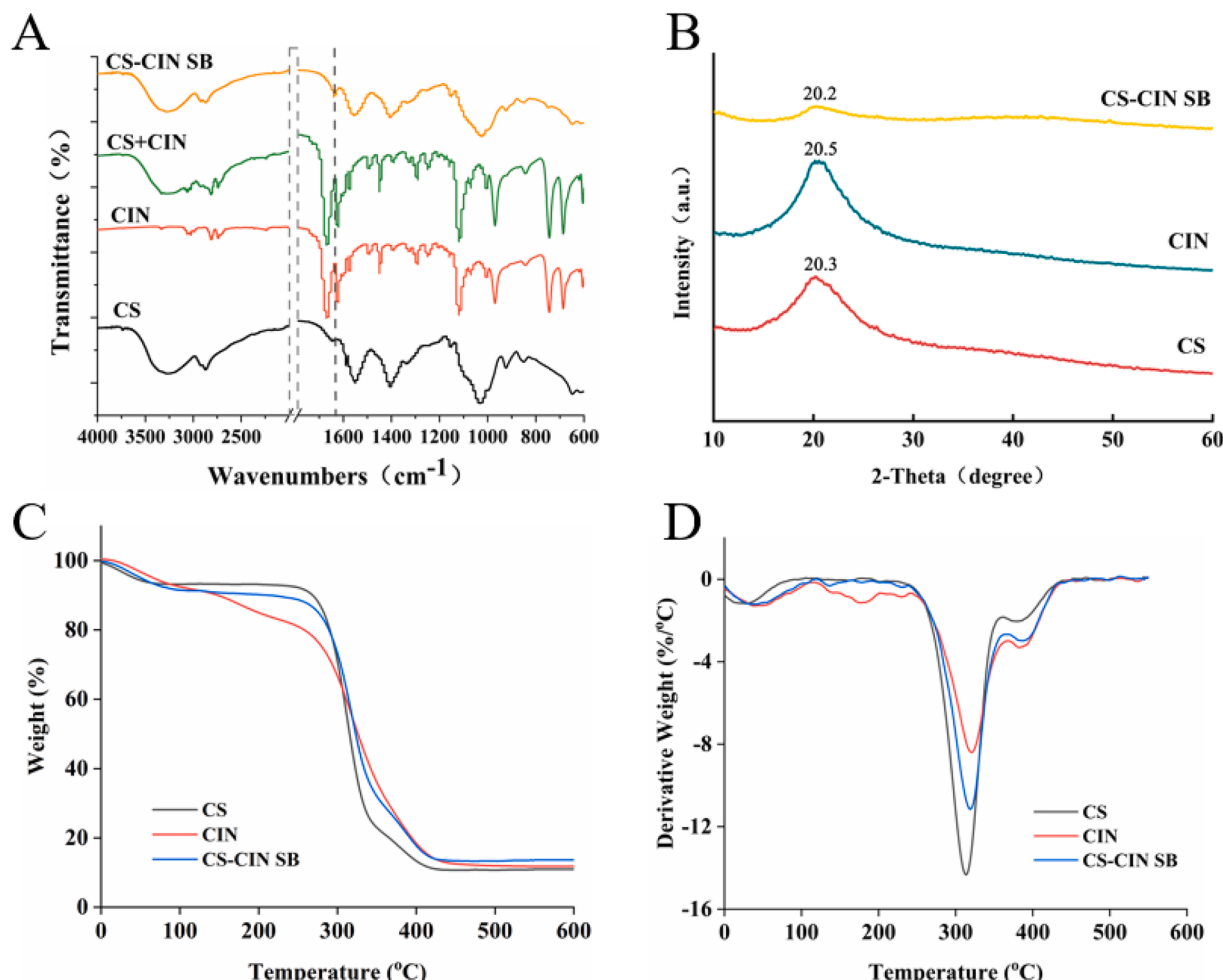


Fig. 3. FTIR spectra (A); XRD patterns (B); TG curves (C) and DTG curves (D) of the CS, CIN, and CS-CIN SB.

spectrum of the CS-CIN SB at 1634 cm^{-1} confirms the formation of imine groups (Heras-Mozos et al., 2022). The FTIR spectrum of the CS-CIN SB showed the characteristic peaks corresponding to the monosubstitution of aromatic rings in CIN and the vibration peaks of olefins at 750 and 650 cm^{-1} ; these peaks were not observed in the FTIR spectrum of the CS. These results suggest that the chitosan-cinnamaldehyde Schiff base harboured the conjugated structure of cinnamaldehyde. Owing to the consumption of the amino group via the Schiff base reaction, the amino group deformation vibration peak at 1597 cm^{-1} disappeared, whereas the stretching vibration peak of the hydroxyl group near 3430 cm^{-1} and the absorption peak of the glycosidic bond in the chitosan backbone at 1088 cm^{-1} exhibited no significant change pre- and post-reaction. Thus, the Schiff base reaction primarily occurred in the amino group of chitosan without disrupting the original backbone structure.

3.4.2. XRD

As shown in Fig. 3B, characteristic chitosan peak was markedly broadened and shifted to 20.3° in the CS diffractrogram, which was owing to an amorphous state during film formation (Khanzada, 2023). After Schiff base modification, the diffraction peak of CS-CIN SB at $20 = 20^\circ$ exhibited irregular broadening and weakened intensity. This indicates a reduction in the number of free amino groups within the chitosan chain segments due to the Schiff base reaction, disrupting molecular ordering and the crystalline state. Additionally, the introduced groups from the Schiff base reaction interfered with the micro-crystalline structure of chitosan, thereby diminishing polymer crystallinity. These findings confirm the chemical interaction between chitosan and cinnamaldehyde, which alters the original hydrogen bonding and crystallisation characteristics, leading to peak broadening and weakening.

3.4.3. TG

The amount of dissipated heat in the CS, CIN, and CS-CIN SB was analysed to explore the discrepancy in thermal stability between chitosan-cinnamaldehyde Schiff base and base material chitosan. Fig. 3C-D illustrates the three distinct stages of the heat-induced weight loss of the films: the initial stage from room temperature to $100\text{ }^\circ\text{C}$ is linked to the evaporation of water within the sample; the second stage from 100 to $350\text{ }^\circ\text{C}$ is associated with the disruption of the molecular structure of the film, leading to more pronounced decomposition in which the pyranose ring structure gradually deteriorates along the polymer main chain, resulting in the release of small molecular fragments (Khan et al., 2024); and the final stage between 350 and $600\text{ }^\circ\text{C}$ involves the degradation of the amine ring structure within the film.

The thermal stability of the CS-CIN SB demonstrated a high heat resistance, whereas the thermal stability of the CIN fell somewhere in between. Upon reaching a mass loss of 50 %, the degradation temperatures for the CS, CIN, and CS-CIN SB were 315 , 323 , and $325\text{ }^\circ\text{C}$, respectively, indicating that the incorporation of cinnamaldehyde and chitosan-cinnamaldehyde Schiff base elevate the degradation temperature of the film. This enhancement was attributed to the hindrance of thermal degradation product diffusion from chitosan by cinnamaldehyde and chitosan-cinnamaldehyde Schiff base, thereby reducing the mass loss during the pyrolysis process. Cinnamaldehyde typically loses weight rapidly around $200\text{ }^\circ\text{C}$ due to volatilization and thermal decomposition (Balaguer et al., 2011). Comparing the TG curves of CIN and CS-CIN SB, the grafted CS-CIN SB exhibited enhanced thermal stability. This result suggests a reactive transformation with chitosan, forming a new physically stable phase that inhibits the thermal loss of cinnamaldehyde.

3.4. Analysis of relaxation characteristics of chilled fresh mutton meat under different preservation film storage conditions via LF-NMR

LF-NMR spectroscopy can be conducted to assess the mobility of water (bound, immobile, and free water) and the proportion of each

water molecule without disrupting the internal structure of the sample, indicating water retention and freshness levels. T_2 values characterise the mobility of water in various states. A longer relaxation time indicates higher water mobility, whereas a shorter relaxation time indicates lower water mobility. Fig. 4A-D illustrates the LF-NMR spectra of the T_2 relaxation times for the CK, CS, CIN, and CS-CIN SB. The spectra show three peaks, labelled Peak 1, Peak 2, and Peak 3, represented by T_{2b} , T_{21} , and T_{22} , respectively, that correspond to bound water (0 – 10 ms), water with limited flowability (10 – 100 ms), and free water (100 – 1000 ms) (Liu et al., 2025). In mutton, bound water (1 – 5 % of total water) is firmly associated with proteins through electrostatic forces. Immobile water, constituting over 90 % of total water, resides within the structured myofibrillar protein matrix. Free water, located extracellularly, is freely mobile and represents the primary source of drip loss (Luan et al., 2025).

Across the four sets of film samples, the relaxation times decline for T_{2b} and T_{21} , which represent two types of water. This trend could be attributed to the initial refrigeration effects driven by microbial activity and chemical alterations, leading to the relaxation of the muscle fibre structure. Consequently, numerous small pores emerged, enhancing the mobility of less flowable water, significantly decreasing both free and less flowable water. Toward the later stages of refrigeration, water evaporation saturated, prompting mutton to reabsorb a portion of evaporated water from the internal packaging environment, indicating increased immobile water content. After days 9–13, the relaxation time for T_{2b} in the mutton samples continued to increase steadily. The bound water peaks split into two, representing strongly and weakly bound water. This suggests that, during this period, the water-holding capacity of mutton muscle fibres decreased owing to refrigeration, leading to the disruption of some hydrogen bonds between water and muscle proteins. Bound water then tends to transform to less flowable water.

Fig. 4A–D show that the initial peak value of the immobile water amplitude for the refrigerated mutton sample was 5664.99 . By day 11, the relaxation time of the CS-CIN SB group was significantly higher than that of the CK group ($P < 0.01$), suggesting that the addition of CIN strengthened the interaction between CIN and proteins, thereby modifying the bonding between the proteins and water molecules and resulting in the formation of free water molecules. Microorganisms in the CK-wrapped sample proliferated more rapidly, leading to changes in the protein side chain groups and a decrease in the strength of binding between the protein and water molecules. Toward the end of the cold storage period, the peak values of the immobile water amplitudes for the CK-, CS-, CIN-, and CS-CIN SB-wrapped samples were 2850 , 3455 , 3786 , and 4454 , respectively. These findings indicate that the immobile water content of the CK-wrapped sample decreased more rapidly as the sampling time was extended in relation to that of the CS-CIN SB-wrapped sample, possibly because the CS-CIN SB-wrapped sample maintained a higher immobile water content. This could be attributed to the inhibition of microorganisms and preservation of muscle fibres through the slow-release effect of the CS-CIN SB.

Magnetic resonance imaging allows additional visualisation of the distribution and movement of water within chilled mutton muscle tissues. In Fig. 4E, the corresponding pseudocolour images of the chilled mutton samples under various headspace packaging conditions are shown throughout the storage period. Typically, the red hue in an image signifies an increased proton density, whereas the blue hue indicates low proton density. Darker shades indicate stronger signals, whereas lighter shades indicate weaker signals (Lian et al., 2023). As the storage duration extended, the luminosity of both sets of images gradually diminished, leading to an uneven distribution of the red region. This variation indicated a gradual reduction in the moisture content of the refrigerated mutton samples and a shift in its distribution, suggesting a decline in the water retention capacity of mutton. Over time, the red region of the mutton MRI image transitioned to yellow and green. This indicates a reduction in the amount of juices within the mutton meat over time, which aligns with the relaxation properties of mutton meat in this study.

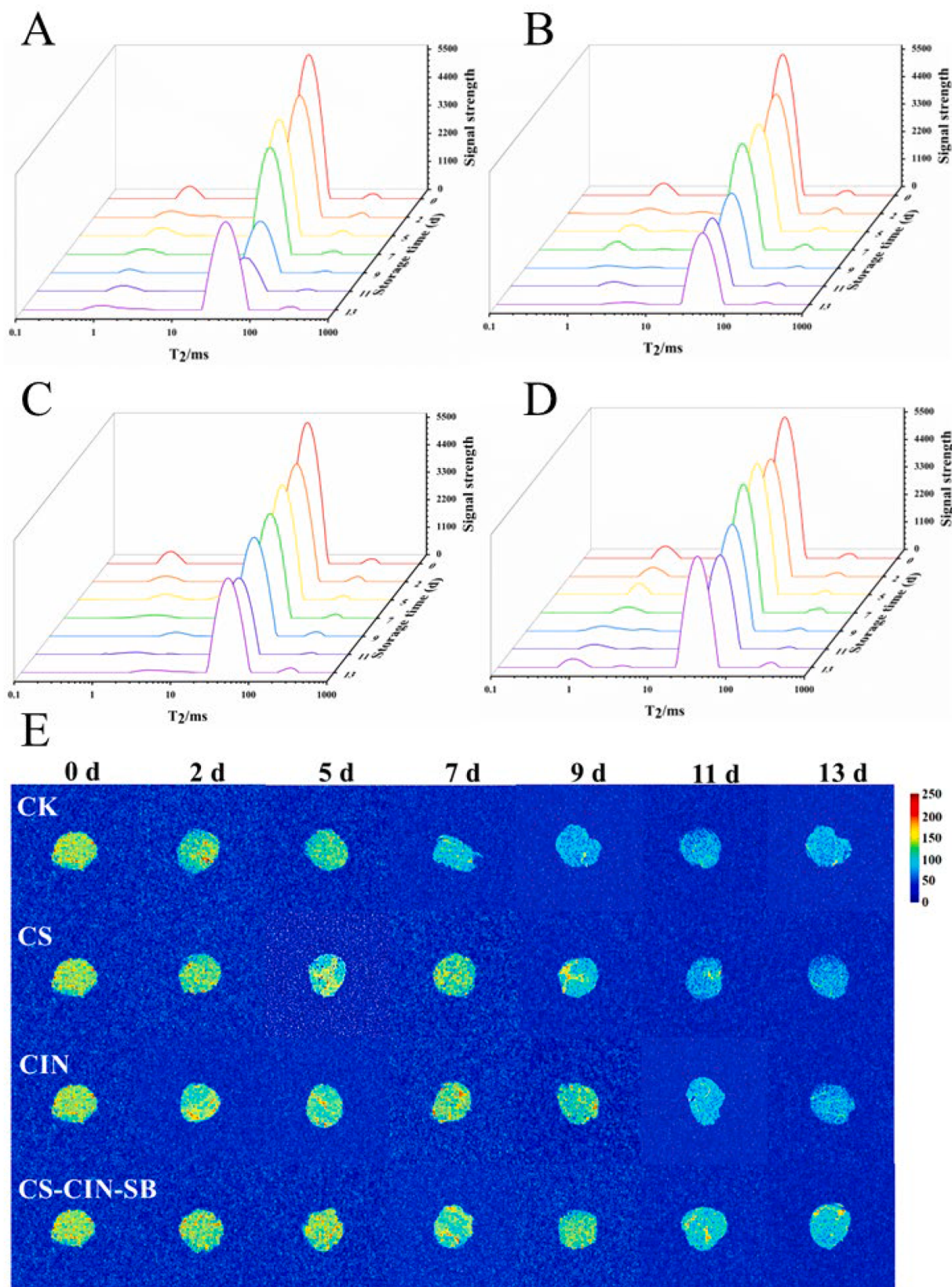


Fig. 4. Analysis of moisture distribution for the mutton meat samples during storage in relation to CK (A); CS (B); CIN (C); and CS-CIN SB (D) and changes in MRI images during the application of four types of films (E).

Initially, the CIN-wrapped mutton sample had higher moisture levels, but subsequently experienced a quicker decline possibly due to the rapid release of cinnamaldehyde, leading to a weakening of the preservative properties of the film with the increase in storage duration. At each sampling point, the CS-CIN SB-wrapped mutton sample consistently had a higher moisture content than the CK-wrapped mutton sample because of the sustained inhibitory effects of cinnamic aldehyde emanating from CS-CIN SB. This result indicates that the antimicrobial film prepared using chitosan-cinnamaldehyde Schiff base effectively delays water migration and allows enhanced water retention. The water retention of the different films is in the order CS-CIN SB > CIN > CS > CK.

3.6. Evaluation of preservation properties of CS-CIN SB-wrapped mutton

3.6.1. Appearance and colour

The changes in mutton sample brightness, represented by L^* , over time during storage under varying film conditions are shown in Fig. 5A. The brightness levels generally declined, but the L^* values of the mutton samples wrapped in the CIN and CK exhibited a slight upward trend by the seventh day of storage. This can be attributed to the continuous proliferation of microorganisms, leading to protein degradation, reduced muscle water retention, and cellular water leakage. Consequently, surface moisture accumulation in mutton meat increased, enhancing light reflection and consequently boosting brightness levels. The L^* values decreased consistently during the storage period. The decline in brightness was more pronounced in the CK-wrapped sample than in the other three film-treated samples from day 0 to day 9, which exhibited some degree of bacteriostatic activity. Overall, the CS-CIN SB-wrapped mutton sample displayed the slowest diminishing trend, suggesting the superior preservation capability of the CS-CIN SB, which is consistent with the observations shown in Fig. 5D.

Fig. 5B shows that the a^* value gradually declined over time during the 13 d storage period. This decrease is attributed to the intricate biochemical reactions that occur as the meat is chilled during storage. At the end of the preservation period, the a^* values for all groups significantly decreased in relation to their initial values ($p < 0.01$), consistent with the results reported by Song (Song et al., 2020). On the 13th day of assessment, the a^* value of the CS-CIN SB-wrapped mutton sample exhibited a highly significant disparity ($p < 0.01$) compared to the CK-wrapped mutton samples. As depicted in Fig. 5C, the b^* values for all four sample groups consistently increased over time, with the b^* value of the CK group reaching 13.70 on day 13, marking the peak value during storage. Furthermore, the impact of diverse storage conditions on mutton b^* values was substantial.

3.6.2. pH

As depicted in Fig. 5E, the pH of the mutton meat samples varied when subjected to different packaging material. After storage at 4 °C, the pH of the mutton meat samples initially declined and then increased. Based on the reference standard for the pH value, the pH range defining first-grade fresh meat is 5.8–6.2, while the pH of second-grade fresh meat ranges between 6.3 and 6.6. Any pH value exceeding 6.7 indicates meat spoilage (Zhao et al., 2022). Analysis of the curve pattern in the graph revealed that the CK-wrapped mutton sample exhibited the most rapid pH increase, suggesting a higher level of mutton spoilage in the CK than in the other three films. By day 11, the CS-, CIN-, and CK SB-wrapped mutton samples met the criteria for second-grade fresh meat classification. In contrast, the pH of the CS-CIN SB-wrapped mutton sample was 6.06, aligning with the first-grade fresh meat standard and thus demonstrating a significant disparity from that of the control film ($p < 0.05$). In general, the CS-CIN SB-wrapped mutton sample exhibited the slowest increase in pH. Even when the control samples reached the spoilage threshold at 13 d (pH=6.65), the CS-CIN SB-wrapped mutton sample remained in the second-grade fresh meat category (pH=6.24), presenting a significant deviation from the other three sample groups ($p < 0.01$). This suggests that the CS-CIN SB

effectively suppressed the growth and proliferation of microorganisms during storage, inducing a notable preservation effect. The trends observed in the CS- and CIN-wrapped mutton samples were similar; however, the pH level of the CS-wrapped mutton sample consistently surpassed that of the CIN-wrapped mutton sample. This indicates that under identical conditions, the addition of cinnamaldehyde induced a superior inhibitory effect on spoilage bacteria.

3.6.3. TBARS

Fig. 5F illustrates that the TBARS values gradually increased over time after slaughter during refrigerated storage. Studies have indicated that when TBARS values exceed 0.5 mg/kg, fat oxidation is accelerated, resulting in a rancid flavour in chilled mutton (Guo et al., 2023). Throughout the storage period, the CS-, CIN-, and CK-wrapped mutton samples attained spoilage thresholds (0.537 mg/kg, 0.537 mg/kg, 0.57 mg/kg) by day 9. The TBARS value of the CS-CIN SB-wrapped mutton sample was 0.376 mg/kg, falling below the minimum spoilage threshold, and the TBARS values on day 9 of storage showed a significant reduction in relation to those of the other film-treated samples ($p < 0.05$). By the 13th day, the TBARS value of the CS-CIN SB-wrapped mutton sample was 0.225 mg/kg lower than that of the CK-wrapped mutton sample ($p < 0.01$). This demonstrates that storage at 4 °C decreased the rate of lipid oxidation and prevented an increase in the TBARS value.

3.6.4. TVB-N

According to the GB2707–2016 standard, the TVB-N content of fresh meat should not exceed 15 mg/100 g. Fig. 5G illustrates the changes in the TVB-N levels during mutton storage, showing a gradual increase in the TVB-N values of samples over time. Additionally, the groups (CS-, CIN-, and CS-CIN SB-wrapped mutton samples) all exhibited spoilage on the 13th day, which was extended by 4 days compared to the CK-wrapped mutton sample. Among them, the CS-CIN SB-wrapped mutton sample demonstrated the greatest effectiveness in delaying protein degradation, thus providing the best preservation effect.

3.6.5. TVC

The accumulation of bacterial colonies escalates with prolonged storage (Fig. 5H). However, the incorporation of bacteriostatic agents into the film tempers the pace of this increase. In the initial two days, there were no notable distinctions among the CS-, CIN-, CS-CIN SB-, and CK-wrapped mutton samples, likely due to the sluggish development and reproduction of microbes in the early storage phase. By day 5, the total colony count of the CK-wrapped mutton sample reached $6.45 \log_{10}$ CFU/g, surpassing the minimum requirement, while the CS- and CIN-wrapped mutton samples exceeded this threshold by day 9, registering $6.41 \log_{10}$ CFU/g and $6.39 \log_{10}$ CFU/g, respectively, signifying the partial inhibitory impact of CS and CIN on spoilage bacteria. Throughout the storage period, the CS-CIN SB-wrapped mutton sample consistently maintained the lowest colony count, thereby prolonging the shelf life of mutton to 13 d with optimal preservation efficacy.

3.6.6. Volatile flavor compounds

The dominant volatiles in fresh mutton were aldehydes, alcohols, and esters. Aldehydes are primarily produced by the oxidation of fats, have low threshold values, strong fruit and flower flavor, and contribute greatly to mutton flavor (Li et al., 2024). Alcohols are produced from the metabolism of sugars, the oxidation of lipids, the decarboxylation of amino acids, and the dehydrogenation of certain compounds (Xu et al., 2025). Although alcohols have a relatively mild effect on the flavor of meat compared to aldehydes, their concurrent presence can markedly influence the overall mutton meat flavor profile. Esters are formed by esterification of alcohols and carboxylic acids in muscle, usually, short-chain esters have a fruity flavor and long-chain esters can impart a fatty flavor to mutton (Guo et al., 2019). As shown in Fig. 6, with the extension of storage time, the content of aldehydes and alcohols (except

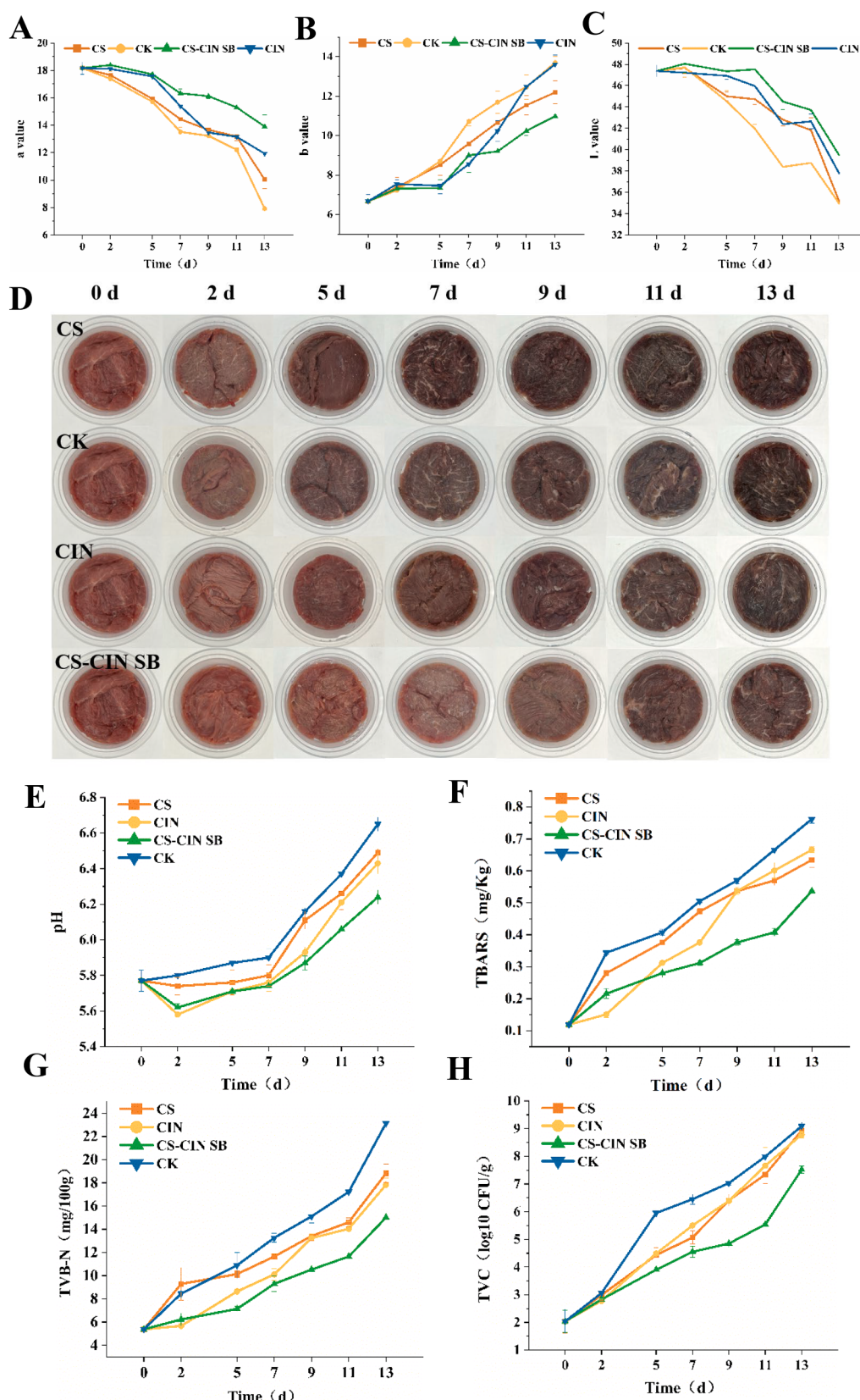


Fig. 5. The a^* (A); b^* (B); and c^* values (C); photographs (D); pH values (E); TBARS values (F); TVB-N values (G) and total viable counts (H) of the mutton samples during storage at 4 °C.

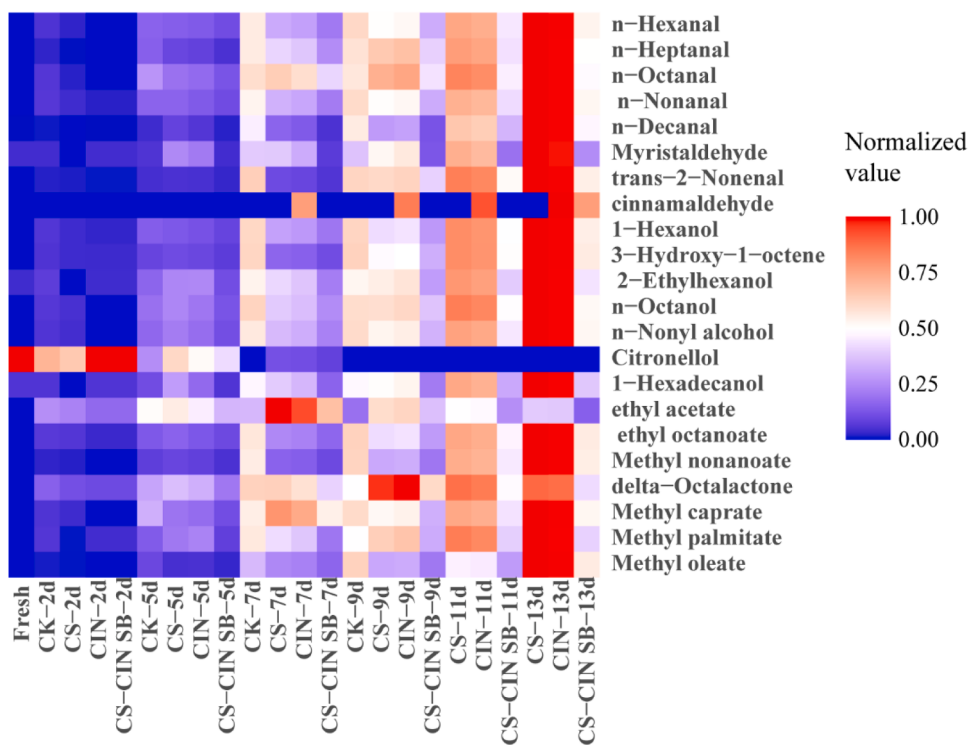


Fig. 6. Heatmap of volatile compounds in the CK-, CS-, CIN-, and CS-CIN SB-wrapped mutton samples.

Citronellol) in the CK-, CS-, CIN-, CS-CIN SB-wrapped mutton samples were increased, the content of esters was first increased and then decreased. Usually, the increase in concentration of aldehydes (e.g., hexanal, octanal, nonanal) can be attributed to the rancid odors or acidification (Yang et al., 2025), excessive alcohols can exhibit a bitter, moldy, and fatty aroma. At the end of storage time, the concentration of aldehydes and alcohols in CS-CIN SB-wrapped mutton sample was lower than that in CK-, CS-, CIN- wrapped samples, indicating that CS-CIN SB can help to prevent the deterioration of mutton flavor. At 13d, a small amount of cinnamaldehyde was detected in the CS-CIN SB-wrapped mutton sample, this result together with TVB-N, TVC, and TBARS data, demonstrates the need for prompt consumption.

4. Conclusions

An antibacterial film with pH-responsive release properties was developed using chitosan-cinnamaldehyde. The addition of cinnamaldehyde substantially improved the mechanical strength and thermal stability of the CS-CIN SB. The as-prepared CS-CIN SB successfully overcame the limitations of volatile and unstable cinnamaldehyde, exhibiting sensitivity to pH changes for controlled release. The freshness of CS-CIN SB-wrapped mutton stored at 4 °C was monitored for 13 days, and CS-CIN SB was found to exhibit strong freshness-preserving capability. The film effectively inhibited the growth of spoilage bacteria, reduced juice loss in chilled mutton, and maintained the colour and appearance of the meat. Additionally, it slowed the increase in mutton pH and TVB-N, extending the freshness of mutton meat by approximately 4 days. The release characteristics aligned with the preservation requirements of chilled mutton, offering a straightforward and promising approach for developing highly effective antibacterial films.

Funding

This work was supported by Key R&D Program of Shandong Province, China (2022TZXD0021& 2023CXGC010712& 2023CXGC010708). China Agriculture Research System (CARS-38).

Modern Agricultural Technology Industry System of Shandong Province (SDAIT-10-09).

Ethical statement-studies in humans and animals

This article does not contain any studies with humans and animals performed by any of the authors.

CRedit authorship contribution statement

Lei Wen: Writing – review & editing, Writing – original draft, Visualization, Investigation, Formal analysis. **Pengfei Du:** Supervision, Conceptualization. **Weiting Wang:** Project administration, Funding acquisition. **Yaobo Liu:** Supervision, Resources, Project administration. **Peng Hu:** Investigation. **Jianfang Cao:** Investigation. **Yanli Ma:** Writing – review & editing, Writing – original draft, Visualization, Project administration, Investigation, Funding acquisition, Formal analysis.

Declaration of competing interest

The authors declare that they have no known competing financial interests or personal relationships that could have appeared to influence the work reported in this paper.

Supplementary materials

Supplementary material associated with this article can be found, in the online version, at doi:10.1016/j.fufo.2025.100757.

Data availability

Data will be made available on request.

References

- Al Ati, G., Chkirate, K., El-Guourrami, O., Chakchak, H., Tüziün, B., Mague, J.T., Essassi, E.M., 2024. Schiff base compounds constructed from pyrazole-acetamide: synthesis, spectroscopic characterization, crystal structure, DFT, molecular docking and antioxidant activity. *J. Mol. Struct.* 1295, 136637.
- Arokiyaraj, S., Dinakarkumar, Y., Shin, H., 2023. A comprehensive overview on the preservation techniques and packaging of processed meat products: emphasis on natural derivatives. *J. King. Saud. Univ. Sci.*, 103032.
- Awad, A.M., Kumar, P., Ismail-Fitry, M.R., Jusoh, S., Ab Aziz, M.F., Sazili, A.Q., 2022. Overview of plant extracts as natural preservatives in meat. *J. Food. Process. Preserv.* 46 (8), e16796, 2022.
- Balaguer, M.P., Gomez-Estaca, J., Gavara, R., Hernandez-Munoz, P., 2011. Functional properties of bioplastics made from wheat gliadins modified with cinnamaldehyde. *J. Agric. Food. Chem.* 59 (12), 6689–6695.
- Batiha, G.E.S., Hussein, D.E., Algammal, A.M., George, T.T., Jeandet, P., Al-Snafi, A.E., Thorat, N.D., 2021. Application of natural antimicrobials in food preservation: recent views. *Food. Control.* 126, 108066.
- Cavalcante, D.N., Corrêa, R.F., Campelo, P.H., Sanches, E.A., Bezerra, J.d.A., 2023. Essential oils from unconventional food plants (*Murraya* spp, *Ocimum* spp, *Piper* spp) as alternative food flavorings. *Food. Chem. Adv.*, 100481.
- Cheng, S., Su, R., Song, L., Bai, X., Yang, H., Li, Z., Lü, X., 2023. Citral and trans-cinnamaldehyde, two plant-derived antimicrobial agents can induce *Staphylococcus aureus* into VBNC state with different characteristics. *Food. Microbiol.* 112, 104241.
- Chen, H., Hu, X., Chen, E., Wu, S., McClements, D.J., Liu, S., Li, B., Li, Y., 2016. Preparation, characterization, and properties of chitosan films with cinnamaldehyde nanoemulsions. *Food. Hydrocoll.* 61, 662–671.
- Culas, M., Popovich, D., Rashidinejad, A., 2023. Recent advances in encapsulation techniques for cinnamon bioactive compounds: A review on stability, effectiveness, and potential applications. *Food. Biosci.*, 103470.
- Dong, J., Yu, D., Zhang, L., Wang, G., Zhang, P., You, Y., Xia, W., 2024. Chitosan/alginate dialdehyde trilayer films with cinnamaldehyde nanoemulsions for grass carp preservation. *Food. Hydrocoll.* 147, 109413.
- Feng, S., Dai, S., Wei, Z., Wang, J., Xiang, N., Shao, P., 2024. Soy conglycinin amyloid fibril and chitosan complex scaffold for cultivated meat application. *Food. Hydrocoll.* 153, 110017.
- Guo, X., Lu, S.L., Wang, Y.Q., Dong, J., Ji, H., Wang, Q.L., 2019. Correlations among flavor compounds, lipid oxidation indices, and endogenous enzyme activity during the processing of Xinjiang dry-cured mutton ham. *J. Food. Process. Preserv.* 43, e14199.
- Guo, Z., Wu, S., Lin, J., Zheng, H., Lei, H., Yu, Q., Jiang, W., 2023. Active film preparation using pectin and polyphenols of watermelon peel and its applications for super-chilled storage of chilled mutton. *Food. Chem.* 417, 135838.
- Hanim, M.A., Nuraini, A., 2022. Characterization of natural bionanocomposites polymers for food packaging. *Bionanocompos. Food. Packag. Appl.* 69–90.
- He, X., Li, M., Gong, X., Niu, B., Li, W., 2021. Biodegradable and antimicrobial CSC films containing cinnamon essential oil for preservation applications. *Food. Packag. Shelf.* 29, 100697.
- Heras-Mozos, R., Hernández, R., Gavara, R., Hernández-Muñoz, P., 2022. Dynamic covalent chemistry of imines for the development of stimuli-responsive chitosan films as carriers of sustainable antifungal volatiles. *Food. Hydrocoll.* 125, 107326.
- Heras-Mozos, R., López-Carballo, G., Hernández, R., Gavara, R., Muñoz, P.H., 2023. pH modulates antibacterial activity of hydroxybenzaldehyde derivatives immobilized in chitosan films via reversible Schiff bases and its application to preserve freshly-squeezed juice. *Food. Chem.* 403, 134292.
- Hou, T., Ma, S., Wang, F., Wang, L., 2023. A comprehensive review of intelligent controlled release antimicrobial packaging in food preservation. *Food. Sci. Biotechnol.* 32 (11), 1459–1478.
- Khan, A., Riahi, Z., Kim, J.T., Rhim, J.-W., 2024. Chitosan/gelatin-based multifunctional films integrated with sulfur-functionalized chitin for active packaging applications. *Food. Hydrocoll.* 149, 109537.
- Khaneghah, A.M., Hashemi, S.M.B., Limbo, S., 2018. Antimicrobial agents and packaging systems in antimicrobial active food packaging: an overview of approaches and interactions. *Food. Bioprod. Process.* 111, 1–19.
- Khanzada, B., Mirza, B., Ullah, A., 2023. Chitosan based bio-nanocomposites packaging films with unique mechanical and barrier properties. *Food. Packag. Shelf.* 35, 101016.
- Kuai, L., 2021. Preparation of Ph-Responsive Cinnamaldehyde-Chitosan Schiff base With Controlled Release Behavior and Its Application in Fruit and Vegetable Preservation. Jiangnan University master thesis.
- Li, X., Wang, Y., Xu, J., Yang, Q., Sha, Y., Jiao, T., Zhao, S., 2024. Effects of yeast cultures on meat quality, flavor composition and rumen microbiota in lambs. *Curr. Res. Food. Sci.* 9, 100845.
- Lian, F., Cheng, J.-H., Ma, J., Sun, D.-W., 2023. LF-NMR and MRI analyses of water status and distribution in pork patties during combined roasting with steam cooking. *Food. Biosci.* 56, 1103325.
- Limbo, S., Ubaldi, E., Adobati, A., Iametti, S., Bonomi, F., Mascheroni, E., Piergiovanni, L., 2013. Shelf life of case-ready beef steaks (Semitendinosus muscle) stored in oxygen-depleted master bag system with oxygen scavengers and CO₂/N₂ modified atmosphere packaging. *Meat. Sci.* 93 (3), 477–484.
- Lin, J., Meng, H., Guo, X., Tang, Z., Yu, S., 2023. Natural aldehyde-Chitosan Schiff base: fabrication, pH-responsive properties, and vegetable preservation. *Foods* 12 (15), 2921.
- Lin, j., Wang, H., Du, P., Wang, W., Liu, Y., Xiong, G., Yu, K., Ma, Y., 2025. Effect of static magnetic field-assisted repeated freezing and thawing on quality characteristics, microstructure, and myofibrillar protein properties of lamb meat. *Innov. Food. Sci. Emerg. Technol.* 104, 104112.
- Liu, J., Liu, S., Chen, Y., Zhang, L., Kan, J., Jin, C., 2017. Physical, mechanical and antioxidant properties of chitosan films grafted with different hydroxybenzoic acids. *Food. Hydrocoll.* 71, 176–186.
- Luan, X., Jin, C., Li, M., Wang, J., Chen, G., Zhang, X., Dong, X., Li, P., 2025. The impact of varying intensity magnetic field-assisted sub-freezing preservation technology on the quality and protein structure of mutton. *LWT-Food. Sci. Technol.* 226, 117968.
- Manzoor, A., Yousuf, B., Pandith, J.A., Ahmad, S., 2023. Plant-derived active substances incorporated as antioxidant, antibacterial or antifungal components in coatings/films for food packaging applications. *Food. Biosci.*, 102717.
- Martínez-Aguilar, V., Peña-Juárez, M.G., Carrillo-Sánchez, P.C., López-Zamora, L., Delgado-Alvarado, E., Gutierrez-Castañeda, E.J., Gonzalez-Calderon, J.A., 2023. Evaluation of the antioxidant and antimicrobial potential of SiO₂ modified with cinnamon essential oil (*Cinnamomum Verum*) for its use as a nanofiller in active packaging PLA films. *Antioxidants* 12 (5), 1090.
- Mills, J., Donnison, A., Brightwell, G., 2014. Factors affecting microbial spoilage and shelf-life of chilled vacuum-packed lamb transported to distant markets: A review. *Meat. Sci.* 98 (1), 71–80.
- Montejar-López, M., Castillo, R., Jiménez, A.J.L., Gómez-Gómez, L., Ahrazem, O., Niza, E., 2024. Polyac saccharide film containing cinnamaldehyde-chitosan nanoparticles, a new eco-packaging material effective in meat preservation. *Food. Chem.* 437, 137710.
- Nadira, P., Mujeeb, V.A., Rahman, P.M., Muraleedharan, K., 2022. Effects of cashew leaf extract on physicochemical, antioxidant, and antimicrobial properties of N, O-Carboxymethyl chitosan films. *Carbohydr. Polym. Technol. Appl.* 3, 100191.
- Negi, H., Verma, P., Singh, R.K., 2021. A comprehensive review on the applications of functionalized chitosan in petroleum industry. *Carbohydr. Polym.* 266, 118125.
- Perdones, Á., Vargas, M., Atarés, L., Chiralt, A., 2014. Physical, antioxidant and antimicrobial properties of chitosan–cinnamon leaf oil films as affected by oleic acid. *Food. Hydrocolloid* 36, 256–264.
- Qin, Y., Liu, Y., Yuan, L., Yong, H., Liu, J., 2019. Preparation and characterization of antioxidant, antimicrobial and pH-sensitive films based on chitosan, silver nanoparticles and purple corn extract. *Food. Hydrocoll.* 96, 102–111.
- Ren, Q.S., Fang, K., Yang, X.T., Han, J.W., 2022. Ensuring the quality of meat in cold chain logistics: a comprehensive review. *Trends. Food. Sci. Technol.* 119, 133–151.
- Ruan, C., Zhang, Y., Sun, Y., Gao, X., Xiong, G., Liang, J., 2019. Effect of sodium alginate and carboxymethyl cellulose edible coating with epigallocatechin gallate on quality and shelf life of fresh pork. *Int. J. Biol. Macromol.* 141, 178–184.
- Smaoui, S., Hlima, H.B., Braiek, O.B., Ennouri, K., Mellouli, L., Khaneghah, A.M., 2021. Recent advancements in encapsulation of bioactive compounds as a promising technique for meat preservation. *Meat. Sci.* 181, 108585.
- Song, W., Du, Y., Yang, C., Li, L., Wang, S., Liu, Y., Wang, W., 2020. Development of PVA/EVA-based bilayer active film and its application to mutton. *LWT-Food. Sci. Technol.* 133, 110109.
- Sun, Y., Zhang, M., Bhandari, B., Bai, B., 2021. Nanoemulsion-based edible coatings loaded with Fennel essential oil/cinnamaldehyde: characterization, antimicrobial property and advantages in pork meat patties application. *Food. Control.* 127, 108151.
- Tagrida, M., Nilsuwann, K., Gulzar, S., Prodpran, T., Benjakul, S., 2023. Fish gelatin/chitosan blend films incorporated with betel (*Piper betle* L.) leaf ethanolic extracts: characteristics, antioxidant and antimicrobial properties. *Food. Hydrocoll.* 137, 108316.
- Tao, Y., Ma, L., Li, D., Tian, Y., Liu, J., Liu, D., 2021. Proteomics analysis to investigate the effect of oxidized protein on meat color and water holding capacity in Tan mutton under low temperature storage. *LWT-Food. Sci. Technol.* 146, 111429.
- Wang, J., Zhao, F., Huang, J., Li, Q., Yang, Q., Ju, J., 2023. Application of essential oils as slow-release antimicrobial agents in food preservation: preparation strategies, release mechanisms and application cases. *Crit. Rev. Food. Sci. Nutr.* 1–26.
- Wang, L., Liu, T., Liu, L., Liu, Y., Wu, X., 2022. Impacts of chitosan nanoemulsions with thymol or thyme essential oil on volatile compounds and microbial diversity of refrigerated pork meat. *Meat. Sci.* 185, 108706.
- Wu, K., Zhang, T., Chai, X., Duan, X., He, D., Yu, H., Tao, Z., 2022. Encapsulation efficiency and functional stability of cinnamon essential oil in modified β-cyclodextrins: in vitro and in silico evidence. *Foods* 12 (1), 45.
- Wu, M., Chen, J., Huang, W., Yan, B., Peng, Q., Liu, J., Zeng, H., 2020. Injectable and self-healing nanocomposite hydrogels with ultrasensitive pH-responsiveness and tunable mechanical properties: implications for controlled drug delivery. *Biomacromolecules* 21 (6), 2409–2420.
- Xie, Q., Liu, X., Zhang, Y., Liu, G., 2023. Development and characterization of a new potato starch/watermelon peel pectin composite film loaded with TiO₂ nanoparticles and microencapsulated *Lycium barbarum* leaf flavonoids and its use in the Tan mutton packaging. *Int. J. Biol. Macromol.* 252, 126532.
- Xu, J., Wang, C., Liu, T., Luo, R., Zheng, C., Zhang, Y., Lang, X., 2025. Meat quality differences and protein molecular mechanisms affecting meat flavor in different breeds of Tibetan sheep analyzed by 4D label-free quantitative proteomics. *Food. Chem.* 480, 143977.
- Yang, Z., Cui, Z., Zhang, M., Sun, L., Zhao, L., Su, L., Jin, Y., 2025. Analysis of the effects of hydroxyl radicals on the volatile flavor composition and lipid profile of sheep meat based on HS-SPME-GC-MS and UPLC-MS/MS studies. *Food. Chem.* 484, 144161.
- Zhang, J., Zhang, J., Huang, X., Shi, J., Muhammad, A., Zhai, X., Zou, X., 2023. Study on cinnamon essential oil release performance based on pH-triggered dynamic mechanism of active packaging for meat preservation. *Food. Chem.* 400, 134030.

- Zhang, M., Sun, L., Su, R., Corazzin, M., Yang, Z., Dou, L., Jin, Y., 2024. Widely targeted metabolomic analysis reveals the dynamic changes of metabolites during postmortem chilled aging in Mongolian sheep. *Food. Chem.* 431, 137035.
- Zhao, W., Li, C., Ma, W., He, R., Rong, Y., Sarker, S., Liu, Q., Tian, F., 2023. A novel active packaging film containing citronella oil: preparation, characterization, antimicrobial activity and application in grape preservation. *Food. Packag. Shelf.* 40, 101168.
- Zhao, Y., Kong, X., Yang, X., Zhu, L., Liang, R., Luo, X., Zhang, Y., 2022. Effect of energy metabolism and proteolysis on the toughness of intermediate ultimate pH beef. *Meat. Sci.* 188, 108798.